JOURNAL OF GEOPHYSICAL RESEARCH, VOL. 101, NO. B12, PAGES 28,189–28,204, DECEMBER 10, 1996

Isothermal flow of an anisotropic ice sheet in the vicinity of an ice divide

Anne Mangeney
Laboratoire de Glaciologie et Geophysique de l'Environnement, CNRS, Saint Martin d'Heres, France

Francesco Califano[1]
Observatoire de Paris-Meudon, Meudon, France

Olivier Castelnau[2]
Laboratoire de Glaciologie et Geophysique de l'Environnement, CNRS, Saint Martin d'Heres, France

Abstract. Simulations of glacier flow are commonly based on the assumption that ice has an isotropic viscosity. Here we examine the plane flow of ice in the special region of an ice divide using a constitutive relation for an anisotropic, incompressible viscous body that is orthotropic and transversally isotropic. Ice is assumed to be isotropic at the ice sheet surface, with the continuous development of a vertical single maximum c axis fabric with increasing depth. We consider the theoretical case of an isothermal ice sheet over a horizontal bedrock, with no slip at the ice-bedrock interface. The ice sheet surface elevation is imposed, and the flow corresponding to the steady state is calculated, using a two-dimensional finite difference model based on the resolution of a pressure-Poisson equation. In this model, all components of the stress and strain rate tensor are calculated. The main conclusion is that for a fixed surface elevation, the general flow pattern accelerates when the anisotropic behavior of the ice is taken into account due to the greater fluidity with respect to shear stress. The downward motion of the ice is faster, despite a higher resistance to vertical deformation. As a result, the dominance of shear strain rate in the flow of polar ice is stronger in the anisotropic case than in the isotropic case. The shear stresses are slightly relaxed, while the longitudinal stresses are significantly increased in the anisotropic case.

1. Introduction

The classical isotropic Norton-Hoff constitutive relation (or "Glen flow law") [*Nye*, 1957] is usually used in ice sheet modeling:

$$\tilde{D_{ij}} = \tilde{B}\tilde{\tau_e}^{n-1}\tilde{S'_{ij}}, \quad \tilde{B} = \tilde{B_0}exp(-Q/R\tilde{T}), \qquad (1)$$

with the effective stress defined as

$$\tilde{\tau_e} = \frac{1}{2}tr\tilde{\mathbf{S}'}^2. \qquad (2)$$

Here $\tilde{D_{ij}}$ and $\tilde{S'_{ij}}$ are the components of the strain rate tensor $\tilde{\mathbf{D}}$ and the symmetric Cauchy stress deviator $\tilde{\mathbf{S}}'$, respectively, Q is the activation energy for creep, R is the gas constant, and $\tilde{T}$ is the absolute temperature.

The value of the exponent n and the rate factor $\tilde{B}$ have been the subject of extensive research [*Hooke*, 1981]. The value of the stress sensitivity n is 3 for equivalent stress higher than about 0.2 MPa. For lower stresses, both mechanical tests and borehole tilt measurements lead to a value lower than 2 [*Doake and Wolff*, 1985; *Pimienta and Duval*, 1987; *Alley*, 1992]. This latter stress condition should prevail in ice sheets. For a given value of n, it is widely accepted that the parameter $\tilde{B_0}$ is a function of the structure of polar ice. However, at the scale of an ice sheet, polar ice cannot be considered as an isotropic material. Observations of deep ice cores clearly show the development of lattice preferred orientations (fabric) with depth.

At the ice sheet surface, c axis orientations are randomly distributed and ice is isotropic. Deeper down, as long as ice temperature is lower than -12^0C, preferred c axis orientations reflect the whole deformation history of ice particles, from the ice sheet surface down to the present depth. Fabric develops mainly as a result of intracrystalline deformation, but the influence of rotation recrystallization (polygonization) on fabric development cannot be neglected [*Alley et al.*, 1995; *Castelnau et al.*, 1996b]. Strongly concentrated single maximum fabrics with c axes orientated toward the in situ vertical direction are generally found, for example, in Byrd [*Gow and Williamson*, 1976], Dye 3 [*Herron et al.*, 1985], GRIP (GReenland Ice core Project)

[1]Now at Scuola Normale Superiore (INFM-FORUM), Pisa, Italy.
[2]Now at LPMTM-CNRS, Université Paris-Nord, Institut Galilee, Villetaneuse, France.

Paper number 96JB01924.
0148-0227/96/96JB-01924$09.00

[*Thorsteinsson et al.*, 1996] and GISP2 (Greenland Ice Sheet Programme 2) [*Anandakrishnan et al.*, 1994] ice cores. More particular fabrics, with c axes concentrated in the in situ vertical plane, have been observed in Vostok [*Lipenkov et al.*, 1989] and Mizuho [*Fujita et al.*, 1987] cores. Above the critical temperature of -12^0C (in basal layers), a regime of dynamic recrystallization with a rapid grain boundary migration rate appears (migration recrystallization), and fabrics reflect the instantaneous stress configuration [*Duval and Castelnau*, 1995]. This latter mechanism leads to multimaxima fabrics as found in the basal layers of the Byrd core [*Gow and Willianson*, 1976]. According to *Lliboutry and Duval* [1985], these ices can be considered, as a first approximation, isotropic. A strong viscoplastic anisotropy of polar ice appears when fabrics become concentrated [*Lile*, 1978; *Russel-Head and Budd*, 1979; *Shoji and Langway*, 1988; *Pimienta and Duval*, 1988; *Budd and Jacka*, 1989]. Indeed, the directional viscosities of a given polycrystal can differ by 2 orders of magnitude depending on the direction of the applied stress. This effect is due to the strong viscoplastic anisotropy of ice crystals, which deform easily only by dislocation glide in the basal plane. When all c axes are concentrated around the vertical direction, polycrystalline ice can deform easily with respect to horizontal shear (all grains are well oriented for a deformation by basal glide) but strongly resists all longitudinal stresses (hard glide orientation).

The influence of the $\tilde{B}_0$ dependence on texture (size and shape of individual crystals), fabric (orientation of crystals lattice), and impurity content on the flow has been investigated in ice sheet modeling by multiplying the isotropic viscosity, in the Norton-Hoff relation, by an ad hoc enhancement factor [*Shoji and Langway*, 1984; *Kostecka and Whillans*, 1988; *Reeh*, 1988; *Dahl-Jensen*, 1985; *Schott et al.*, 1992; C. Schott Hvidberg et al., Ice flow between the GRIP and GISP2 boreholes in Central Greenland, submitted to *Journal of Geophysical Research*, 1996]. Results obtained in this way suggest that the use of a flow law derived from laboratory studies on isotropic ice to model flow in regions where natural ice masses exhibit strong anisotropy would underestimate the actual shear rates by 1 order of magnitude [*Lile*, 1978]. However, while the effect of the texture may be represented with a scalar factor $\tilde{B}_0$, the influence of the fabric, which introduces a directional effect in the polycrystal response, has to be investigated using a viscosity tensor.

The question of how a realistic anisotropic flow law (i.e., describing both the behavior of polycrystalline ice as it is found in polar ice sheets and the evolution of this behavior with deformation history) may influence the flow has not be dealt with until now. This is essentially due to two difficulties.

The first difficulty is to find an adequate anisotropic constitutive relation, which suitably describes the behavior of polar ices in large deformations and which can be easily implemented into a large-scale flow model. Micro-macro models, in which polycrystal behavior is derived from the average behavior of grains, can be used to calculate the behavior of polar ice when the strain history is known [*Azuma*, 1994; *Castelnau and Duval*, 1994; *Van der Veen and Whillans*, 1994; *Castelnau et al.*, 1996a]. However, the introduction of such a model in an ice sheet flow model requires large computer capacity, since the storage of the orientation angles of at least 100 grains is necessary at each grid point. Furthermore, such micro-macro models should take into account the effects of dynamic recrystallization processes, which are not well understood, to correctly reproduce the natural fabric development [*Van der Veen and Whillans*, 1994; *Castelnau et al.*, 1996b]. A reasonable first step is then to use an analytical constitutive relation that does not calculate fabric development with strain history but that gives the anisotropic response of polycrystalline ice for a given fabric. After a preliminary work of *Lile* [1978] and *Andermann* [1982], *Lliboutry and Duval* [1985], and *Lliboutry* [1993] have developed such a constitutive relation for anisotropic, orthotropic, transversally isotropic ice polycrystals, with nonlinear viscosities. Lliboutry's law will be used in this work. This constitutive relation is based on a homogenization theory, assuming a uniform stress state within the polycrystal. It corresponds to the well-known Reuss-type lower bound [*Hutchinson*, 1976] for the viscosity. According to *Castelnau* [1996], the uniform stress model gives a good estimation of the experimental response of anisotropic ice samples but sligthly underestimate the anisotropy. Note that owing to the difficulty of providing accurate mechanical tests on anisotropic ice samples, Lliboutry's relation, which assumes a particular distribution of lattice orientations, has not been completely tested.

The second difficulty lies in the fact that the introduction of an anisotropic flow law in ice sheet models leads to a complex set of dynamic equations. Here we shall consider the effect of the anisotropic behavior of ice in the vicinity of the ice divide, where the full mechanical problem has to be dealt with. Flow modeling of large grounded ice sheets is usually based on the shallow ice approximation [*Hutter*, 1983; *Morland*, 1984]. This assumption significantly simplifies the set of dynamic equations but cannot be used in the region near the ice divide, where the longitudinal stresses and their gradients have to be taken into account [*Szidarovsky et al.*, 1989]. Numerical simulations, treating the full mechanical problem in the vicinity of ice divides, have been carried out over recent years for the case of an isothermal ice sheet on a horizontal bed deforming in plane strain [*Raymond*, 1983] and with an uneven bedrock, variation of temperature with depth and deformation transverse to the direction of flow [*Paterson and Waddington*, 1984; *Schott Hvidberg*, 1996; C. Schott Hvidberg et al., submitted manuscript, 1996]. *Reeh* [1988] has estimated the flow near an ice divide, neglecting the longitudinal stress variations, and bounded the error of his calculated velocities by 30%. *Szidarovsky et al.* [1989] provide a solution including the longitudinal stretching effects, constructed with the aid of a marching procedure by starting at the ice divide. This procedure is based on a prescribed form of the vertical velocity at the

ice divide. These terms have been also calculated using an iterative procedure starting from the shallow ice approximation [*Dahl-Jensen*, 1989a,b]. We use here a different approach, similar to that proposed by *Patankar* [1980]. In our model, all stress and strain rate components are accurately calculated. This allows us to dealt with, for the first time, the case of the flow of anisotropic ice on the scale of an ice sheet.

This paper addresses the question of how the anisotropy of polycrystalline ice, as it is found in polar ice sheets, may change the general pattern of the flow. We shall concentrate on the theoretical case of a two-dimensional (2-D), isothermal, steady state, gravity-driven, viscous, anisotropic, and non-Newtonian flow of ice in an ideal symmetric ice ridge over a rigid bed, subject to surface accumulation. The ice sheet is assumed to be cold (i.e., below the melting point) so that the usual no-slip boundary condition applies at the ice-bedrock interface and the surface elevation is imposed. The work consists of two parts, one adapting the anisotropic constitutive relation developed by Lliboutry to the particular flow case described above, and the other using this constitutive relation in an ice flow model. Effects of anisotropy on stress, pressure, and velocity fields will be discussed. Results will also be compared to those obtained by *Raymond* [1983]. In this preliminary study, only results corresponding to the case of Newtonian behavior ($n = 1$) will be presented.

The paper is structured as follows: first, the equations of the model, second, formulation of the Lliboutry's constitutive relationship for the case of 2-D, symmetric flow and determines the typical evolution of the rheological parameters with depth, third, description of the numerical method for solving the complete set of equations, and finally, the results for $n = 1$.

2. Description of the Problem

2.1. Field Equations

We investigate the behavior of steady, isothermal ice sheet flow by solving the mass balance and momentum equations of a viscous, anisotropic, non-Newtonian fluid. All the dimensional variable are indicated by a tilde. The dynamic pressure $\tilde{p}'$ is calculated from the fluid pressure $\tilde{p}$:

$$\tilde{p}' = \tilde{p} - \rho g \tilde{z}$$

where g is the gravity acceleration, ρ is the characteristic ice density, and $\tilde{z}$ is the vertical coordinate with the origin of the $\tilde{z}$ axis at the bottom. Values of physical parameters are given in Table 1. The deviatoric stress tensor $\tilde{\mathbf{S}}'$, function of the stress tensor $\tilde{\sigma}$, is given by

$$\tilde{\mathbf{S}}' = \tilde{\sigma} + \tilde{p}\mathbf{I}, \quad \tilde{p} = -\frac{1}{3}\mathrm{tr}(\tilde{\sigma})$$

where "tr" is the trace operator and $\mathbf{I}$ is the identity tensor.

We eliminate dimensions from the equations in a way similar to that proposed by *Morland* [1984]. We introduce two characteristic quantities: (1) ice depth d_* and (2) ice velocity u_*. Values of both u_* and d_* are indicated in Table 1; u_* corresponds to a typical accumulation rate of the snow at the upper free surface. The deviatoric Cauchy stress tensor $\mathbf{S}'$ and dynamic pressure p' are scaled by $s_* = \rho g d_*$ (i.e., $\tilde{\mathbf{S}}' = s_* \mathbf{S}', \tilde{p}' = s_* p'$). The mass balance and momentum equations can be written

Table 1. Simulation Parameters

	Description
Physical Parameters	
$\rho = 900$ kg m^{-3}	ice density
$g = 9.81$ m s^{-2}	gravity acceleration
$Q = 7.820 \times 10^4$ J mol^{-1}	activation energy
$R = 8.314$ J mol^{-1} K^{-1}	gas constant
Scaling values	
$u_* = 0.2$ my^{-1}	typical vertical velocity or accumulation rate
$d_* = 2500$ m	representative thickness

$$\nabla.\mathbf{u} = 0, \tag{3}$$

$$\nabla.\mathbf{S}' = \nabla p', \tag{4}$$

where $\mathbf{u} = (u_x, u_z)$ is the dimensionless velocity vector.

The balance laws (3) and (4) are complemented by the constitutive relation of the ice:

$$\mathbf{S}' = \mathbf{M} : \mathbf{D} \tag{5}$$

where $\mathbf{M}$ and $\mathbf{D}$ denote the dimensionless fourth-order viscosity tensor and strain rate tensor, respectively, and colon denotes the twice contracted tensorial product. Strain rate and viscosity components are scaled by u_*/d_* and $s_* d_*/u_*$, respectively. Relation (5) is given explicitly below. All the variable cited further are dimensionless.

2.2. Cartesian Coordinates and Plane Flow

Here we consider a 2-D slab geometry with x and z as the dimensionless horizontal and vertical coordinates. The equations of the top and basal surfaces are

$$z = E(x) \quad \text{(top)}; \quad z = B(x) \quad \text{(bottom)},$$

respectively. The flat basal surface is given by $B(x) = 0$, and the surface elevation profile E is given by

$$E(x) = h_0 - \frac{\beta_0}{2}x^2, \tag{6}$$

where $h_0 = 1.110$ is the height of the ice divide ($x = 0$). The parameter β_0 defines the curvature of the surface profile; calculations were done using several surface elevation profiles, changing the coefficient β_0. A value $\beta_0 = 0.550 \times 10^{-3}$ was selected in order to have a surface elevation profile that leads to a relatively uniform vertical velocity u_z along the surface. The ice sheet geometry is shown shematically in Figure 1. The length of the domain is taken as $L = 40$. $L/2$ is sufficiently

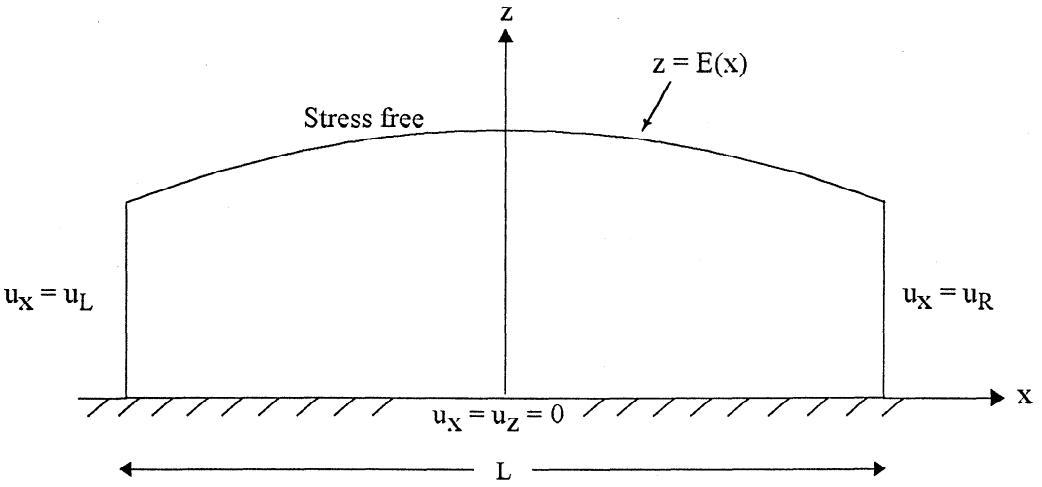

Figure 1. Idealized cross section of two-dimensional symmetric ice divide.

large such that assumptions concerning the details of the variation of velocity with depth on the left- and right-hand boundaries do not affect the solution near the divide [*Raymond*, 1983].

The plane $(x - z)$ is assumed to be a symmetry plane for the flow of the ice sheet. This condition requires that

$$\frac{\partial p'}{\partial y} = D_{yy} = S'_{xy} = S'_{yz} = 0. \tag{7}$$

Note that the only y component of the deviatoric stress occurring in the dynamic equations (4) is S'_{yy}. The projection of equation (4) in the y direction becomes $\partial_y(S'_{yy}) = \partial_y p' = 0$, which is identically satisfied with the present assumptions.

2.3. Boundary Conditions

First, we shall assume that the fluid is at rest at the undeformable base and that the top surface is stress free. Therefore, if $\mathbf{n}_s$ is the exterior unit normal vector at the surface, we have at $z = B(x)$

$$\mathbf{u} = \mathbf{0}, \tag{8}$$

and at $z = E(x)$

$$\sigma.\mathbf{n}_s - p_{\text{atm}}\mathbf{n}_s = 0 \tag{9}$$

where p_{atm} is the atmospheric pressure. Furthermore, still at the upper surface $z = E(x)$, the kinematic surface equation reads

$$u_x \frac{\partial E}{\partial x} - u_z = a \tag{10}$$

where a is the accumulation rate. Equations can be solved by imposing either the accumulation rate [*Schott et al.*, 1992] or the surface elevation [*Raymond*, 1983]. We have chosen the latter condition for the sake of comparison with Raymond's results. In this case, surface velocities and the linked accumulation rate are obtained from both the incompressibility (3) and the stress free condition at the top surface (9). We will then compare the isotropic and anisotropic flow for a given surface elevation. The isotropic and anisotropic flow will then be both in steady state with different accumulation rate.

At the left- and right-hand side of the domain, boundary conditions for the horizontal velocity must satisfy the mass balance,

$$F = \int_\Gamma a(x)dx = \int_{B_R}^{E_R} u_x(x_R, z)dz - \int_{B_L}^{E_L} u_x(x_L, z)dz$$

where F represents the horizontal flux out of the domain, L, R are the left and right edge of the domain, respectively, and Γ is the upper part of the domain. Boundary conditions derived from simple assumptions can be applied at distant boundaries where the detailed form of the boundary condition does not affect the flow at the divide [*Waddington et al.*, 1985]. The depth profile of the horizontal velocity we impose at x_R and x_L is that given by *Nye* [1952], corresponding to laminar flow in an isothermal ice sheet assuming Glen's flow law with exponent n for isotropic ice:

$$u_x(x_M, z) = \frac{1}{2}\left(\frac{n+2}{n+1}\right)\frac{F}{H}\left[1 - \left(\frac{E-z}{H}\right)^{n+1}\right]_{x=x_M}, \tag{11}$$

where $H = E - B$ is the ice thickness and $M = L, R$. Note that no profiles of vertical velocity at M are imposed. We have verified that the solution near the ice divide $(-10 < x < 10)$ is not affected by the different profiles of the horizontal velocity at the boundaries. Even unrealistic profiles lead to the same solution, with a boundary layer near the two edge of the domain.

3. Constitutive Relation

A rate formulation of the plastic deformation can be generated by means of dual dissipation potentials $\psi(\mathbf{D})$ and $\phi(\mathbf{S}')$ [*Ziegler*, 1977; *Hill*, 1987; *Lemaitre and Chaboche*, 1990; *Van Houtte*, 1994]. The knowledge of the

dissipation potential ϕ at the polycrystal scale (macroscopic scale) completely determines the constitutive relation of the polycrystal:

$$D_{ij} = \frac{\partial \phi}{\partial S'_{ij}}, \tag{12}$$

In the case of power law viscosities, the macroscopic potential ϕ is of homogeneus degree $(n+1)$ in the S'_{ij} and reads

$$\phi = \frac{1}{n+1}\dot{W}, \tag{13}$$

where $\dot{W} = S'_{ij}D_{ij}$ represents the rate of plastic work per unit volume. The macroscopic potential can be either assumed to have a particular form [e.g., *Hill*, 1987; *Van Houtte*, 1994] or can be determined from the dissipation potential of individual grains (microscopic scale) by means of a homogenization method. This latter method presents the advantage to be build on more physical considerations. *Andermann* [1982], *Lliboutry and Duval* [1985], and *Lliboutry* [1993] have applied this method to polar ices presenting orthotropic, transversally isotropic behavior. Lliboutry has expressed analytically the macroscopic dissipation potential as well as the value of all rheological parameters. This constitutive relation will be used in the present work.

For the purpose of introducing the notation and the physical concepts, let us briefly recall Lliboutry's evaluation of the constitutive relation. We will then fit the rheological coefficients to the problem under consideration that of a tranversally symmetric plane ice flow.

3.1. Formulation

Lliboutry [1993] assumes that ice crystals deform only by dislocation glide on basal planes. Both mechanical tests and in situ velocity measurements favor two values of the stress exponent of the macroscopic constitutive relation: $n = 1$ for small stress and $n = 3$ for large stress [*Lliboutry and Duval*, 1985; *Doake and Wolff*, 1985; V. Lipenkov et al., Bubbly ice densification in ice sheets: Applications, submitted to *Journal of Geophysical Research*, 1996]. Lliboutry assumes then that the macroscopic dissipation potential is of the form $\phi = P_2(S'_{ij}) + P_4(S'_{ij})$, with P_2 and P_4 denoting homogeneous polynomials of the S'_{ij} with degrees 2 and 4, respectively. This macroscopic potential is given by the volume average of the individual dissipation potential ϕ_c of each grain. This microscopic potential is taken as

$$\phi_c = \frac{1}{2}\psi_b \tau_b^{\,2} + \frac{1}{4}B_b \tau_b^{\,4}, \tag{14}$$

where τ_b is the resolved shear stress on the basal plane. The coefficients ψ_b and B_b a priori depend on the fabric of the polycrystal.

Lliboutry [1993] assumes that the deviatoric stress is uniformly distributed in the polycristal. According to *Lliboutry and Duval* [1985], this uniform stress bound may be applicable to polar ices since the slow grain boundary migration is an efficient accomodation processus. The consequence of this assumption is described in detail by *Castelnau et al.* [1996a] and *Castelnau* [1996]. We will now explicit the analytical form of ϕ.

It is more convenient to derive the potential (equation (12)) in a space where all the stress components S'_{ij} are independent. Second-order symmetrical tensors which have a trace equal to zero display only five independent components and can therefore be represented by vectors in a 5-D space. This is the case for the deviatoric stress $\mathbf{S}'$, and for the strain rate tensor $\mathbf{D}$ if the ice is assumed to be incompressible. Any arbitrary convention for contracting the tensor components into vector components may be used, as long as stress and strain rate are work conjugated [*Canova et al.*, 1985]:

$$\dot{W} = S'_{ij}D_{ij} = S'_k D'_k, \quad (i,j = 1,3; k = 1,5). \tag{15}$$

The symmetries of the constitutive relation directly depend on fabric symmetries, which are closely linked to those of the deformation history [*Canova et al.*, 1985]. In polar ice sheets, the deformation history of an ice particule is complex and then does not present any symmetries. However, natural fabrics usually present a concentration of c axes around the in situ vertical direction and the fabric is approximatively circular [*Thorsteinsson et al.*, 1996; *Anandakrishnan et al.*, 1994]. We will then consider, as a first approximation, that the in situ vertical axis $(z'z)$ is a revolution axis for the fabrics. Thus it is assumed that ice is orthotropic and transversally isotropic in the $(x-y)$ plane, where y is the direction transversal to the flow. This assumption requires any scalar function of the S'_i to be invariant either by a rotation of the Cartesian frame of reference about the z axis, or when the x and y axes are inverted. These symmetries leave a single degree of freedom in a 5-D space and provide four invariants. Lliboutry's analysis is valid for a general 3-D ice flow; let us consider here the special case of a 2-D flow. The invariants reads

$$\begin{aligned} &S'_{ax} = \sqrt{3}/2 S'_{zz} \\ &\tau_\perp^2 = (2S'_{xx} + S'_{zz})^2/4 \\ &\tau_\parallel^2 = {S'_{xz}}^2 \\ &K_3 = (2S'_{xx} + S'_{zz}){S'_{xz}}^2/2. \end{aligned} \tag{16}$$

The expression of ϕ becomes

$$\begin{aligned} \phi \;=\; & \frac{1}{2}[\psi_{ax}{S'_{ax}}^2 + \psi_\perp \tau_\perp^2 + \psi_\parallel \tau_\parallel^2] \\ & + \frac{1}{4}[B_{ax}{S'_{ax}}^4 + B_\perp \tau_\perp^4 + B_\parallel \tau_\parallel^4 + 2A_{\perp\parallel}\tau_\perp^2\tau_\parallel^2 \\ & + 2A_{\parallel ax}\tau_\parallel^2{S'_{ax}}^2 + 2A_{ax\perp}{S'_{ax}}^2\tau_\perp^2 - 4\sqrt{3}C S'_{ax}K_3], \end{aligned}$$

where $(\psi_i,\ B_j,\ A_{kl},\ C)$ are 10 rheological parameters. The ψ_i are proportional to ψ_b, while B_j and A_{kl} are proportional to B_b.

Inverting relation (12) and using (7), we obtain a constitutive equation for orthotropic, transversally isotropic ice, giving the components M_{ijkl} of the symmetrical viscosity tensor:

$$\begin{bmatrix} S'_{xx} \\ S'_{yy} \\ S'_{zz} \\ S'_{xz} \end{bmatrix} = \begin{bmatrix} M_1 & M_6 & M_5 & 0 \\ M_6 & M_2 & M_4 & 0 \\ M_5 & M_4 & M_3 & 0 \\ 0 & 0 & 0 & M_7 \end{bmatrix} \begin{bmatrix} D_{xx} \\ D_{yy} \\ D_{zz} \\ D_{xz} \end{bmatrix} \quad (17)$$

where

$$\begin{aligned} M_1 = M_{xxxx} &= \gamma(\varphi_{ax} - 3CS'^2_{xz}) \\ M_2 = M_{yyyy} &= \gamma(\varphi_{ax} + CS'^2_{xz}) \\ M_3 = M_{zzzz} &= \gamma(\varphi_{\perp} - CS'^2_{xz}) \\ M_4 = M_{yyzz} &= -\gamma(\varphi_{\perp} + 3CS'^2_{xz}) \\ M_5 = M_{xxzz} &= \gamma(-\varphi_{\perp} + CS'^2_{xz}) \\ M_6 = M_{xxyy} &= -\gamma(\varphi_{ax} + CS'^2_{xz}) \\ M_7 = M_{xzxz} &= 4\lambda \end{aligned}$$

and where $\gamma = 1/(\varphi_{ax}\varphi_{\perp} - 3C^2S'^4_{xz})$ and $\lambda = 1/(2\varphi_{\parallel} - 3C(2S'_{xx} + S'_{zz})S'_{zz})$. The three scalar fluidities are defined as

$$\begin{bmatrix} \varphi_{ax} \\ \varphi_{\perp} \\ \varphi_{\parallel} \end{bmatrix} = \begin{bmatrix} \psi_{ax} \\ \psi_{\perp} \\ \psi_{\parallel} \end{bmatrix} + \begin{bmatrix} B_{ax} & A_{ax\perp} & A_{\parallel ax} \\ A_{ax\perp} & B_{\perp} & A_{\perp\parallel} \\ A_{\parallel ax} & A_{\perp\parallel} & B_{\parallel} \end{bmatrix} \begin{bmatrix} S'^2_{ax} \\ \tau^2_{\perp} \\ \tau^2_{\parallel} \end{bmatrix}. \quad (18)$$

This constitutive equation is a direct consequence of *Lliboutry*'s [1993] work, but to the best of the author's knowledge, it has never been written nor used in this form. It is worth pointing out that in the anisotropic case, even if the deformation is planar (i.e., $D_{yy} = 0$), the tranversal stress S'_{yy} is not generally equal to zero. Note that for the special case of material symmetries we consider here, any longitudinal deformation rate, D_{xx}, D_{zz} will produce only longitudinal stresses, S'_{xx}, S'_{zz}, while a shear deformation rate D_{xz} results only in a shear stress component S'_{xz}.

3.2. Rheological Parameters

In the case of axial symmetry around the z axis, the macroscopic potential ϕ depends only on ψ_b, B_b and on the distribution of the angles θ between the c axis of each grain and the z axis.

In these study we make four main simplifications:

1. The coefficients ψ_b and B_b are independent of the fabric. The reason for this simplification is that no relation has been proposed in the litterature. L. Lliboutry (personal communication, 1996) speculates that B_b should increase with the fabric strengthening, which should increase the density of mobile dislocations. For Newtonian viscosity, the number of mobile dislocations is independent of the stress [*Lliboutry and Duval*, 1985]. It is then resonnable to take ψ_b independent of the fabric.

2. The fabric is described by a function $V(\theta)$ of distribution of c axes orientation; $V(\theta)$ represents the volume of grains for which the angle between the c axis and the in situ vertical direction is larger than θ. *Lliboutry* [1993] takes $V(\theta) = \cos^{\nu}\theta$, where the exponent ν expresses the strengthening of the fabric.

3. Fabrics, and then also all rheological parameters, are considered as fixed at each grid point; i.e., they are not updated with the strain history. We will then compare the flow of isotropic and anisotropic ice masses, where the rheological parameters are imposed.

4. The recrystallized basal ice layer, as usually observed in natural ice sheets and which is roughly isotropic, is not taken into account in our theoretical calculation.

B_b and ψ_b are fitted to reproduce the behavior of isotropic ice given by *Budd and Jacka* [1989] for $n = 3$ and *Castelnau et al.* [1996a] for $n = 1$. Here ψ_b and B_b are scaled by $u_*/(\tau_* d_*)$ and $u_*/(d_*\tau_*^3)$, respectively. The resulting dimensionless values are, at -20^0C:

$$\psi_b = 1.42 \times 10^4 \quad ; \quad B_b = 2.31 \times 10^9.$$

The 10 rheological coefficients can then be expressed as a function of a parameter $\theta_{1/2}$, which is linked to the exponent ν by the relation

$$\nu = \frac{-\ln 2}{\ln(\cos\theta_{1/2})}$$

and which verify $V(\theta_{1/2}) = 1/2$; $\theta_{1/2} = 60^0$ for isotropic ice and a zero value corresponds to the case where all c axes align exactly with the in situ vertical direction. The fabric development used here is assumed to be a function of the reduced depth:

$$\theta_{1/2} = \alpha\left(\frac{z-E}{H}\right)^2 + \beta\left(\frac{z-E}{H}\right) + \theta_0 \quad (19)$$

with $\alpha = 49.5$, $\beta = 99$ and $\theta_0 = 60^0$. The coefficients α, β, and γ have been fitted on the fabric data of the recent GRIP ice core [*Thorsteinsson et al.*, 1996] that represent a typical fabric distribution found in ice sheets. Then $\theta_{1/2}$ decreases from 60^0 at the ice sheet surface (isotropic ice) to about 10^0 near the bedrock (strongly preferred vertical c axis orientation). The Schmid diagrams corresponding to the fabric described by (19) are shown at four equidistant depths from the surface to the bottom (Figure 2). This fabric is assumed to be invariant in the horizontal direction.

At the ice sheet surface we obtain

$$\psi_i = \frac{2}{5}\psi_b;\ B_i = A_{ij} = \frac{8}{35}B_b;\ C = 0\ (i,j = ax, \perp, \|)$$

At the bottom, B_{ax}, $B_{\perp}$, $A_{ax\perp}$, and $\psi_{\perp}$ are at least 1 order of magnitude lower than their corresponding values at the surface. Values of $A_{\|ax}$, $A_{\perp\|}$, and ψ_{ax} decrease by factors of 3.4, 1.3, and 3.4, respectively, from the surface down to the bedrock. On the other hand, $B_{\|}$ and $\psi_{\|}$ increase by factors of 3.6 and 2.2. $B_{\|}$ and $\psi_{\|}$ both determine the directional fluidity of the ice with respect to a shear stress S'_{xz}.

Owing to incompressibility (3), the 2-D flow law may be expressed as

$$\begin{aligned} S'_{xx} &= \eta_{xx}D_{xx} \\ S'_{zz} &= \eta_{zz}D_{zz} \\ S'_{xz} &= \eta_{xz}D_{xz} \end{aligned} \quad (20)$$

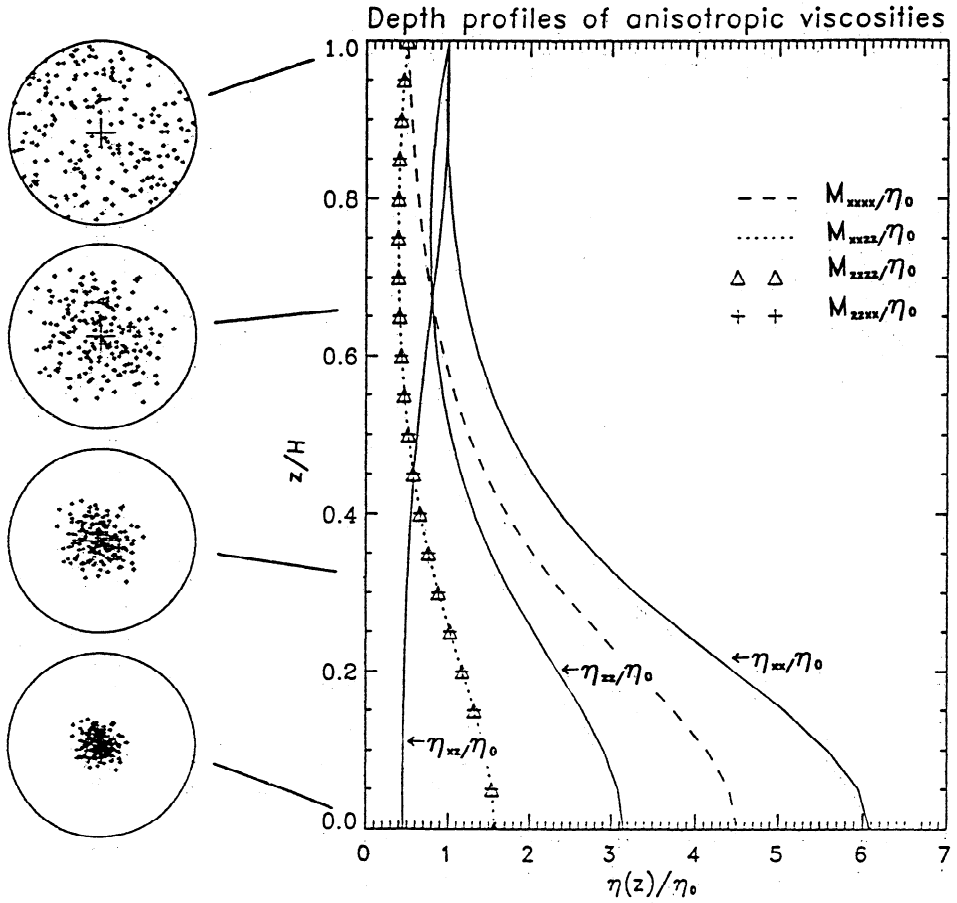

Figure 2. Characteristic of the fabric used in the model and the associated directional viscosities. (left) Ice crystals orientation fabrics described by equation (19) at 0, 1/4, 1/2, 3/4 and 1 times the depth. (right) The directional viscosities resulting from this fabric. The viscosity tensor components are various symbols and the viscosities (η_{ij}) defined in equation (20) are solid lines.

where $\eta_{xx} = M_{xxxx} - M_{xxzz}$, $\eta_{zz} = M_{zzzz} - M_{zzxx}$, and $\eta_{xz} = M_{xzxz}$ are directional viscosities.

In the present work, the numerical application treats only the case of Newtonian viscosity ($n = 1$, B_b=0). Note in that case, all coefficients B_i, A_{ij} and C are equal to zero. For linear flow, all three viscosities (η_{ij}) are independent on the stress. At the surface, they are equal to the isotropic viscosity $\eta_0 = 5/\psi_b$. The vertical profiles of these viscosities, induced by the fabrics and normalized by η_0, are shown in Figure 2. Values of (η_{ij}) are plotted by solid lines, and values of (M_{ijkl}) are plotted by dotted lines or with symbols. It can be seen, at the lower part of the ice sheet that the resistance η_{xx} to horizontal stress S'_{xx} is 1 order of magnitude higher than the resistance to shear stress, while resistance η_{zz} to vertical stress S'_{zz} is half that to horizontal stress.

4. Numerical Method

The numerical solution of the steady incompressible Navier-Stokes equations has been the subject of much research. A commonly used approach is the artificial compressibility method [*Chorin*, 1967] where a new term, a pressure time derivative, is inserted into the continuity equation. This artificial pressure is only a numerical artifact, so that the resulting equation has no physical meaning until a steady state is reached. Another possible approach is to start from the unsteady incompressible equations and let the system relax until a steady state is reached. In this case, in general, the continuity equation is replaced by an elliptic pressure-Poisson equation, which can be easily obtained by taking the divergence of the momentum equation. We use here a slightly different approach which is very similiar to the one known as the projection method [*Peyret and Taylor*, 1983; *Patankar*, 1980]. First, an intermediate velocity field is calculated from the momentum equation; then we calculate the pressure in such a way that the velocity field at the new time is divergence free in order to avoid the accumulation of the compressible part of the discretization error. Finally we correct the velocity with the gradients of the pressure obtained in this way.

Equation (4) together with (17) and (3) can be written as

$$\mathcal{L}\mathbf{u} = \nabla p', \qquad \nabla \cdot \mathbf{u} = 0, \tag{21}$$

where $\mathcal{L}$ is a second-order differential operator. We solve the following fictitious time dependent system of equations:

$$\frac{\partial \mathbf{u}}{\partial t} = \mathcal{L}\mathbf{u} - \nabla p', \qquad \nabla \cdot \mathbf{u} = 0, \tag{22}$$

until a steady state is reached. More precisely, we assume that all fields (velocity, pressure, etc.) are known at time step m and split $\mathcal{L}$ into its diagonal $\mathcal{L}_d$ and nondiagonal $\delta\mathcal{L}$ parts:

$$\mathcal{L} = \mathcal{L}_d + \delta\mathcal{L}.$$

We first calculate an intermediate step for the velocity:

$$\hat{\mathbf{u}} = \frac{\alpha^+}{\alpha^-}\mathbf{u}^{(m)} + \frac{\Delta t}{\alpha^-}\delta\mathcal{L}\mathbf{u}^{(m)}. \tag{23}$$

where $\alpha^{\pm} = 1 \pm \Delta t\mathcal{L}_d/2$. The actual velocity field at time $m+1$ is calculated as

$$\mathbf{u}^{(m+1)} = \hat{\mathbf{u}} - \frac{\Delta t}{\alpha^-}\nabla p'^{(m)}, \tag{24}$$

where the pressure $p'^{(m)}$ is obtained by solving the Poisson equation

$$\nabla.\left(\frac{\Delta t}{\alpha^-}\right)\nabla p'^{(m)} = \nabla \cdot \hat{\mathbf{u}}, \tag{25}$$

which is obtained by imposing $\nabla \cdot \mathbf{u}^{(m+1)} = 0$ in equation (24). Equation (25) is solved using standard numerical techniques for the inversion of a banded matrix.

Notice the implicit formulation for the diagonal part $\mathcal{L}_d$ of the operator $\mathcal{L}$ which gives more stability to the temporal scheme as compared to the purely explicit case, allowing the use of larger time steps Δt.

The ways to discretize the operator $\mathcal{L}$ and the continuity equation have been the subject of much investigations in the recent years [*Tafti*, 1995; *Sotiropoulos and Abdallah*, 1991]. We use here a staggered grid in the horizontal direction and a collocated grid in the vertical direction. The horizontal velocity and pressure are separated by $\Delta x/2$ in space, while in the vertical direction all the fields are calculated on the same grid. This discretization did not lead to the appearance of numerical waves.

Furthermore, we transform the domain into a rectangle in the (ζ, ξ) plane [*Hindmarsh and Hutter*, 1988], using the transformation

$$\zeta = x; \qquad \xi = \frac{z - E}{H}.$$

The equations are then discretized using this coordinate transformation. The finite difference solution scheme is second-order accurate.

The code has been tested in a simplified geometry and compared with analytical solutions for many different initial conditions, time step increments, and spatial resolutions [*Mangeney*, 1996]. Within the numerical domain, the solution for both the isotropic and anisotropic case does not depend on the boundary conditions for the horizontal velocity at the left and right sides of (11). This result is similar to that of *Raymond* [1983]. This independence occurs in the region $-10 < x < 10$. The following results are shown in this domain.

5. Results

We consider here the simplest case of a Newtonian fluid ($n = 1$) and of a horizontal bedrock ($B(x) = 0$). Owing to the symmetry of the flow, the results are shown only in the domain corresponding to positive values of x ($0 < x < 10$).

The main observation resulting from the comparison betweeen isotropic and anisotropic flow is the acceleration of the general pattern of the flow when the anisotropic behavior of the ice is taken into account. The greater fluidity with respect to shear stress globally accelerates the flow, and the downward motion of the ice is faster, despite a higher resistance to vertical deformation. This effect may be seen in the vertical and horizontal velocities in the strain rate and stress profiles as well as in the heat produced during the deformation, as discussed below.

5.1. Surface Velocity

The surface velocities along the flow line are shown in Figure 3. In Figures 3a and 3b the anisotropic velocities are plotted as solid lines, while isotropic velocities are dashed-dotted lines. The accumulation rate is drawn in Figure 3c for the isotropic (dashed-dotted lines) and the anisotropic (solid lines) case. Figure 3c shows that the fixed surface elevation requires a value of the accumulation rate more than 1.5 higher in the anisotropic case than in the isotropic case. Indeed, the flow, essentially induced by shear strain rate, is accelerated by the easiness of the response to shear stress induced by the existing fabric. A higher accumulation rate is then required so that the surface elevation reachs its imposed profile. This effect dominates over the increased resistance to vertical stresses which would lower the vertical velocity for the anisotropic case. This conclusion has to be confirm with results of flow modeling in steady state with an imposed accumulation rate in isotropic and anisotropic case. Both horizontal and vertical velocities are then higher in the anisotropic case. As a result, the horizontal surface velocity is increased by a factor of 1.7 compared to the isotropic situation, and the vertical surface velocity is increased by a factor of 1.8. These factors depend on the choice of the c axis distribution (19).

5.2. Velocity Versus Depth

Figure 4 shows computed profiles of horizontal (Figure 4a) and vertical (Figure 4b) velocities for both the isotropic (dotted lines) and anisotropic (solid lines) cases. They are normalized by the corresponding surface values in order to compare profiles at different longitudinal positions x. Triangles represent the results obtained by *Raymond* [1983] for Newtonian flow.

The results of our model for the isotropic case are in very good agrement with those of Raymond for both u_x and u_z. Profiles at different distance from the ice divide

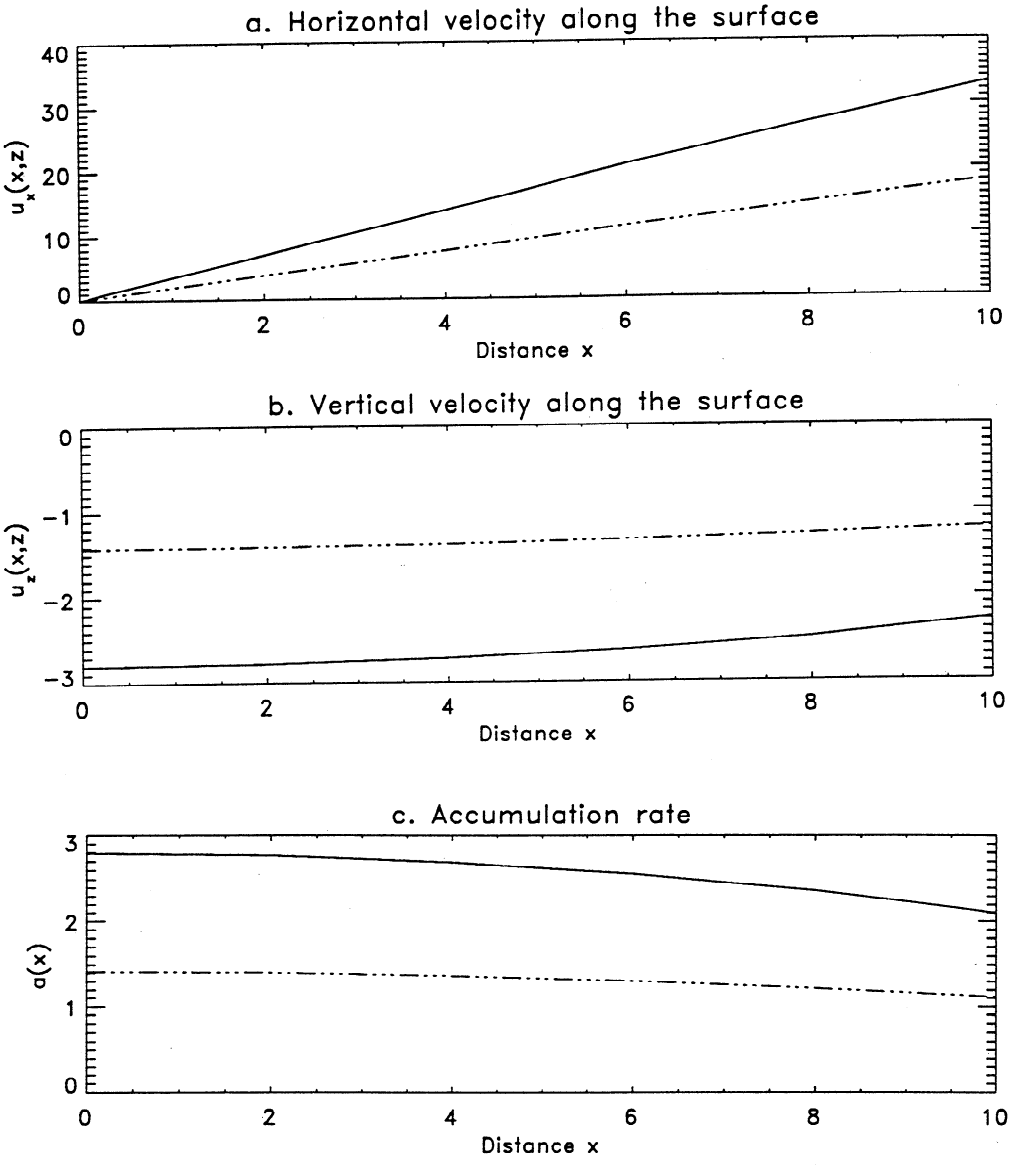

Figure 3. (a) Horizontal and (b) vertical surface velocity profiles. Dashed-dotted lines show surface velocities in the isotropic case and solid lines those in the anisotropic case. (c) The accumulation rate in both the isotropic (dashed-dotted lines) and anisotropic (solid lines) case.

are drawn, but are not distinguable. It is seen, as was pointed out by *Raymond* [1983], that profile shapes are not sensitive to the distance from the divide for $n = 1$ in the isotropic case. The same result is obtained for the case of anisotropic viscosity. However, this conclusion is limited to the case where the fabric pattern is invariant in the horizontal direction. The profile of the downward velocity is more linear in the anisotropic case. The longitudinal strain rates are therefore slightly more uniformly distributed over depth in the anisotropic case. While the shape of vertical velocity is not really affected by the anisotropic nature of ice, the horizontal velocity profiles have a significantly higher curvature. The shearing is then more concentrated in the lower part of the ice sheet.

5.3. Strain Rate and Deviatoric Stress Versus Depth

As proposed by *Raymond* [1983], the results for strain rate are shown in units of

$$\epsilon^* = 2 \mid u_z(0, E) \mid / E(0) \tag{26}$$

and for deviatoric stress in corresponding units of

$$\tau^* = \eta_0 \epsilon^*. \tag{27}$$

Both ϵ^* and τ^* are dimensionless. Note that contrary to Figure 4, where velocities were normalized by their surface value, we use here the same normalization factor for the isotropic and for the anisotropic case. In the

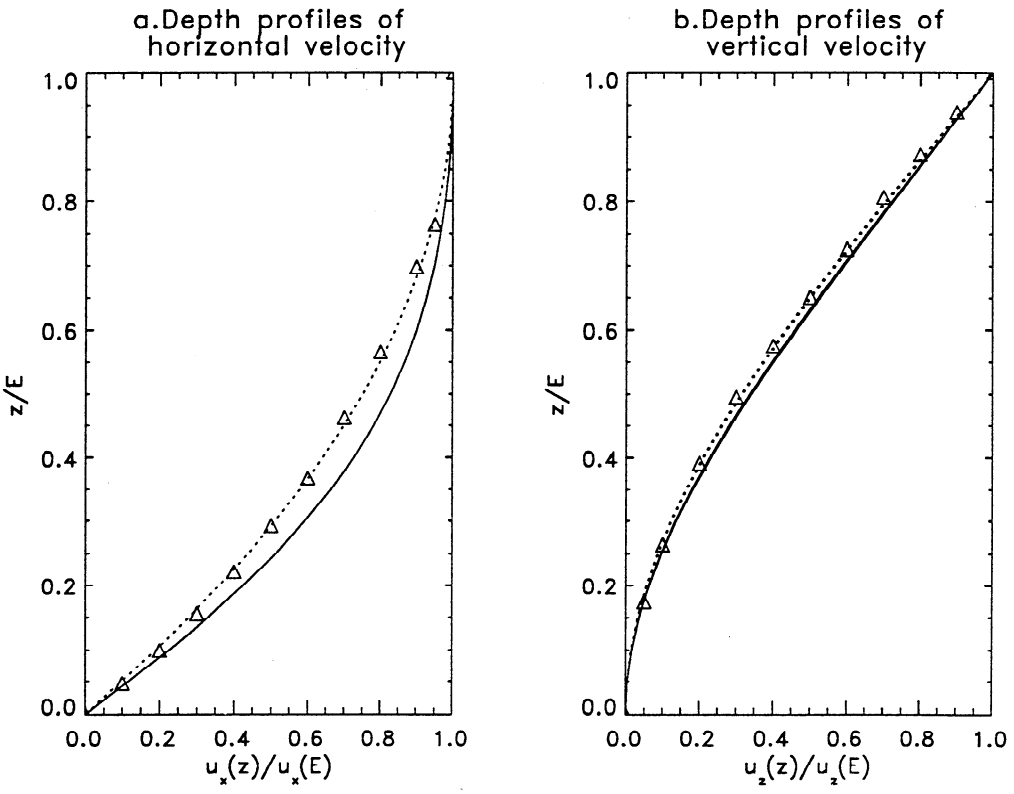

Figure 4. (a) Horizontal and (b) vertical velocity profiles, normalized with respect to their corresponding surface value, versus normalized depth. Solid lines show results of the simulation for the anisotropic case, and dashed lines show those for the isotropic case. Triangles show *Raymond*'s [1983] results for flow of a linear fluid ($n = 1$). The profile shapes are not sensitive to the distance from the divide.

anisotropic case, the normalized strain rate (d_{kl}) and deviatoric stress (s_{kl}), plotted in Figures 5 and 6, are given by

$$(d_{xx}, d_{zz}, d_{xz}) = (D_{xx}, D_{zz}, D_{xz})/\epsilon^*$$
$$(s_{xx}, s_{zz}, s_{xz}) = (S'_{xx}, S'_{zz}, S'_{xz})/\tau^*. \quad (28)$$

The corresponding values in the isotropic case are specified with an exponent i (d^i_{kl} and s^i_{kl}).

The strain rate and deviatoric stress profiles at the ice divide and at $x = 10$ are shown in Figure 5a and 5b, respectively. Globally, deformation rates and axial stresses are larger in the anisotropic case (solid lines) than in the isotropic case (dashed-dotted lines). This is a result of the fact that, as mentioned before, the flow is globally accelerated for a given surface elevation.

It is worth pointing out that, contrary to the isotropic case, where necessarily $s_{xx} = -s_{zz}$, the horizontal stress s_{xx} is higher than the vertical stress s_{zz} in the anisotropic case due to the increased resistance to horizontal stress with respect to vertical stress at the base of the ice sheet (see Figure 2). However, $d_{xx} = -d_{zz}$ in both the isotropic and anisotropic situations demonstrating the incompressibility. The shapes of axial stresses s_{xx} and s_{zz} are completely modified in the case of anisotropic ice. In the upper 1/10 th of the ice sheet, where the ice is nearly isotropic, s_{xx} and s_{zz} decrease with depth under both isotropic and anisotopic conditions. In the lower parts, these stress components increase with depth in the anisotropic case to reach a maximum at $z \sim 1/4$, where the fabric is strongly concentrated. Then they decrease sharply to match the no-slip condition at the base of the ice sheet. Note the significant decrease of both s_{xx} and s_{zz} with the value of x in the lower part of the ice sheet. This effect is greatly reduced in the isotropic case. This is partly due to the fact that the high longitudinal viscosities η_{xx} and η_{zz} in the anisotropic case amplify significantly the stress response to the decrease of the longitudinal strain rate d_{xx} and d_{zz} with x. In fact, the value of the longitudinal strain rate at the surface decreases by a factor of 0.8 in the isotropic case from the ice divide to $x = 10$, while it decreases by a factor of 0.85 in the anisotropic case. The longitudinal strain rate d_{xx} is higher in the anisotropic case both at the ice divide and at $x = 10$. Moreover, the surface longitudinal strain rate at the ice divide is 1.85 times higher in the anisotropic situation and 1.75 times at $x = 10$. The decrease of longitudinal strain rate with x is then faster in the anisotropic case. This partially explains the sharp decrease of s_{xx} and s_{zz} with x in the anisotropic case. At the divide and at half depth, the longitudinal strain rate is 2 times higher in the anisotropic case. At the ice divide the ratio between longitudinal strain rate for the anisotropic and isotropic case increases from 1.85 at the surface to

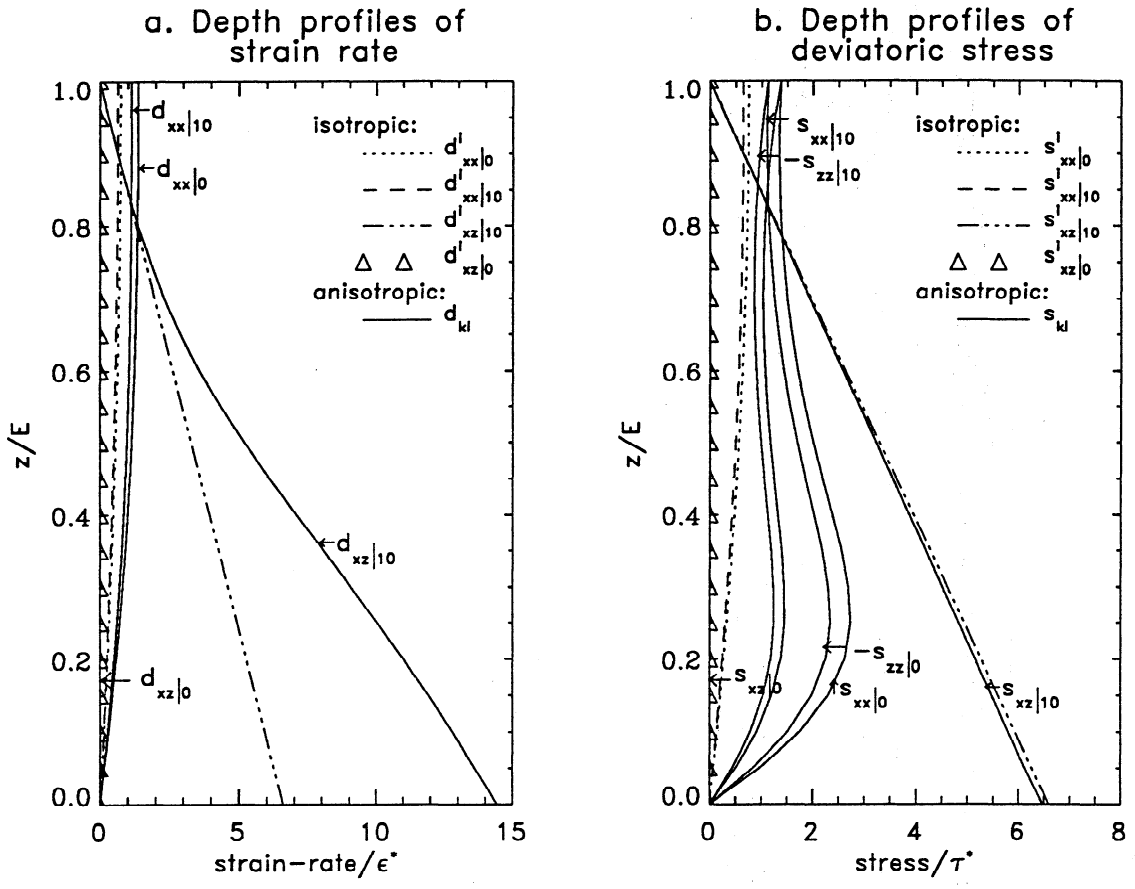

Figure 5. (a) Strain rate and (b) deviatoric stress, normalized by ϵ^* and τ^*, respectively, versus normalized depth. Solid lines show strain rate and stress for the anisotropic case, and symbols represents those for the isotropic case. Numbers (0, 10) indicate the distance from the divide.

2 at half depth. This shows that the distribution of longitudinal strain rate is significantly different in the anisotopic case, as was already apparent in the vertical velocity profile.

Let us now look at the shear components of deviatoric stress and strain rate. At the ice divide, we have $s_{xz} = d_{xz} = 0$ for both anisotropic and isotropic cases. At $x = 10$, it is seen that the shear stress is lowered in the anisotropic case (solid lines) compared to the isotropic case (dashed-dotted lines) but only by a few percent. The low shear resistance relaxes slightly the shear stress s_{xz}. The effect of the anisotropy is more apparent when looking at the shear strain rate. The value of this strain rate at the base of the ice sheet and at $x = 10$ is increased by a factor of 2.2 in the anisotropic case compared to the isotropic case. At $z = 1/2$, this factor is about 1.5. This corroborates the fact that, as mentioned before, shear strain rates are more concentrated in the lower layer for the anisotropic case. This latter factor is not sensitive to the distance from the ice divide. Figure 6 shows the depth profiles of strain rate at distance of 0, 2, 4, and 6 from the ice divide. The shear strain rate in the isotropic and anisotropic case are drawn with dashed-dotted and solid lines, respectively. The maximum value of longitudinal strain rate (i.e., the value at the ice divide) is shown in both the isotropic (dashed lines) and anisotropic (dotted lines) situation. It is seen, in the anisotropic case, that even at a distance of 4 from the divide, the value of the shear strain rate at the base is 4.3 times higher than the maximum value of longitudinal strain rate (i.e., at the surface, at the ice divide). In the isotropic case, this ratio is only 3.5. Therefore it may be concluded that the anisotropic behavior of the ice reduces the domain where the motion of ice is still essentially due to longitudinal strain rate. As mentioned before, the longitudinal strain rate at the divide is 1.85 times higher at the surface in the anisotropic case than in the isotropic case, while the basal shear strain rate is already more than 2 times higher at $x = 2$. In the isotropic case, the basal shear strain is 1 order of magnitude higher than the surface longitudinal strain rate at $x \sim 10$; in the anisotropic case this arises even at $x \sim 8$. As a result, the dominance of shear strain rate in the flow of polar ice is stronger in the anisotropic case than in the isotropic case, for the same isotropic ice at the surface.

The dimensionless effective stress τ_e (scaled by s_*) divided by τ^* is shown in Figure 7 for both the isotropic (Figure 7a) and anisotopic (Figure 7b) cases from the divide to $x = 10$ and from the surface to the bottom. Note that the effective stress τ_e is higher at the surface in the anisotropic case due to the increase of longitu-

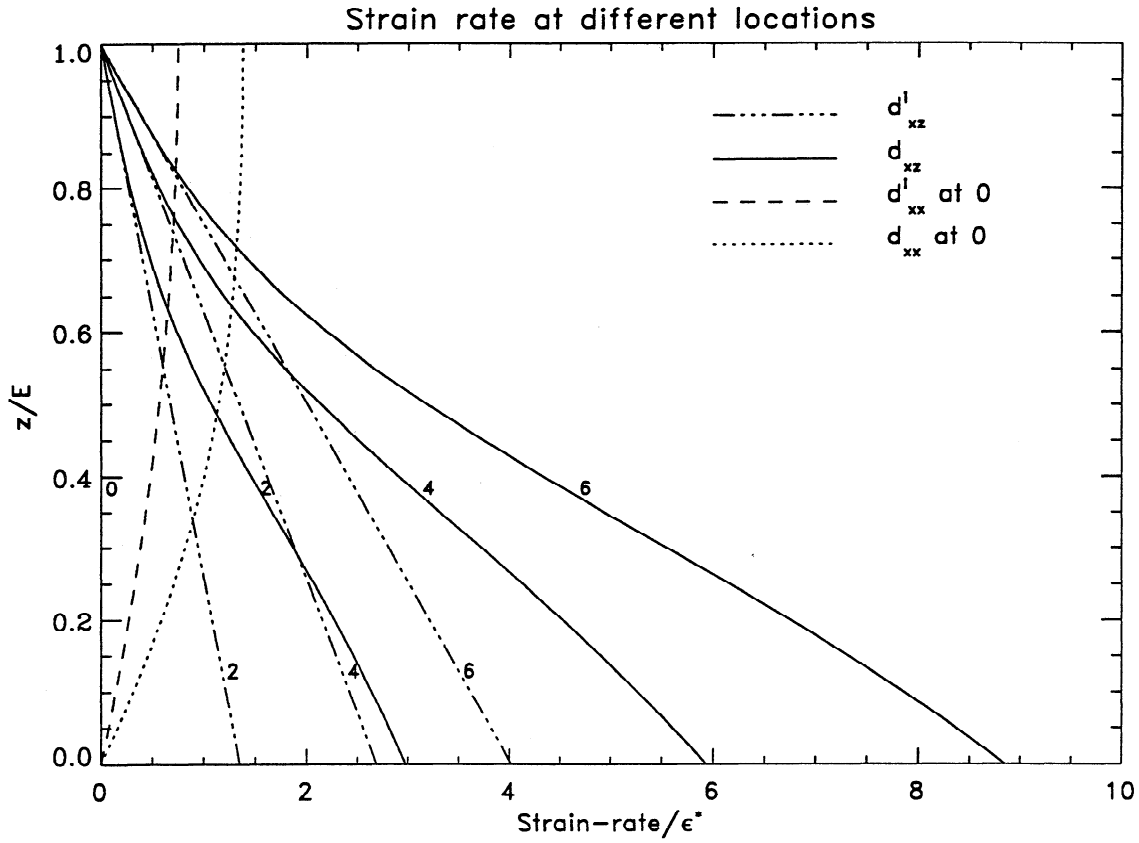

Figure 6. Strain rate, normalized by τ^*, at 0, 2, 4 and 6, respectively. Solid lines show shear strain rate for the anisotropic case (d_{xz}), and dashed-dotted lines show shear strain rate for the isotropic case (d^i_{xz}). Dotted lines show longitudinal strain rate at the divide (where longitudinal strain rate is maximum) for the anisotropic case (d_{xx}), and dashed lines show longitudinal strain rate at the divide for the isotropic case (d^i_{xx}).

dinal stresses. In this case a change of curvature in the vertical profile of τ_e occurs with a maximum at a depth $z \sim 1/4$. Furthermore, the gradient of τ_e in the anisotropic case is very sharp in the lower layers of the ice sheet. These effects diminish with the distance from the ice divide. In the case of a non-Newtonian flow law, the viscosities are stress dependent; we expect therefore a larger influence of the anisotropy on the flow.

Finally, the region of the ice divide, where longitudinal strain rate predominates, is reduced due to the higher dominance of shear strain rate in the anisotropic case than in the isotropic case. However, the characteristic shape of τ_e near the ice divide in the anisotropic case leads to increase the specificity of this region. A nonlinear flow simulation is required to examine thoroughly these considerations.

5.4. Viscous Dissipation of Heat

At the ice divide, where no deformation occurs at the base, the plastic work per unit volume is equal to zero at the bottom (see Figure 8). At the surface, the heat produced by internal deformation is more than 3 times higher in the anisotropic case. However, this surface value is 8 times lower than that obtained at the base of the ice sheet at $x = 4$ in the anisotropic situation. At $x = 4$, the plastic work is already higher at the base than at the surface. This heating will decrease the viscosity at the base of the ice sheet, where shear strain rate dominates and will also contribute to accelerate the flow of polar ice. Therefore the introduction of the heat equation for the temperature should amplify the concentration of the deformation at the base of the ice sheet and amplify the effect of the anisotropy. However, the global flow acceleration will increase the advection of cold ice from the surface down to the bottom. The resulting increase of the viscosity will then reduce the acceleration of the flow in a coupled thermo-mechanical ice sheet model. This speculation have to be verify with the calculation of the temperature field, while the heat dissipation in a location does not affect directly the viscosity in this location but does affect the local thermic balance.

6. Conclusion

The main results for the comparison between isotropic and anisotropic flow are as follows, for a given isotropic ice at the surface, a given fabric development with depth, and a given surface elevation:

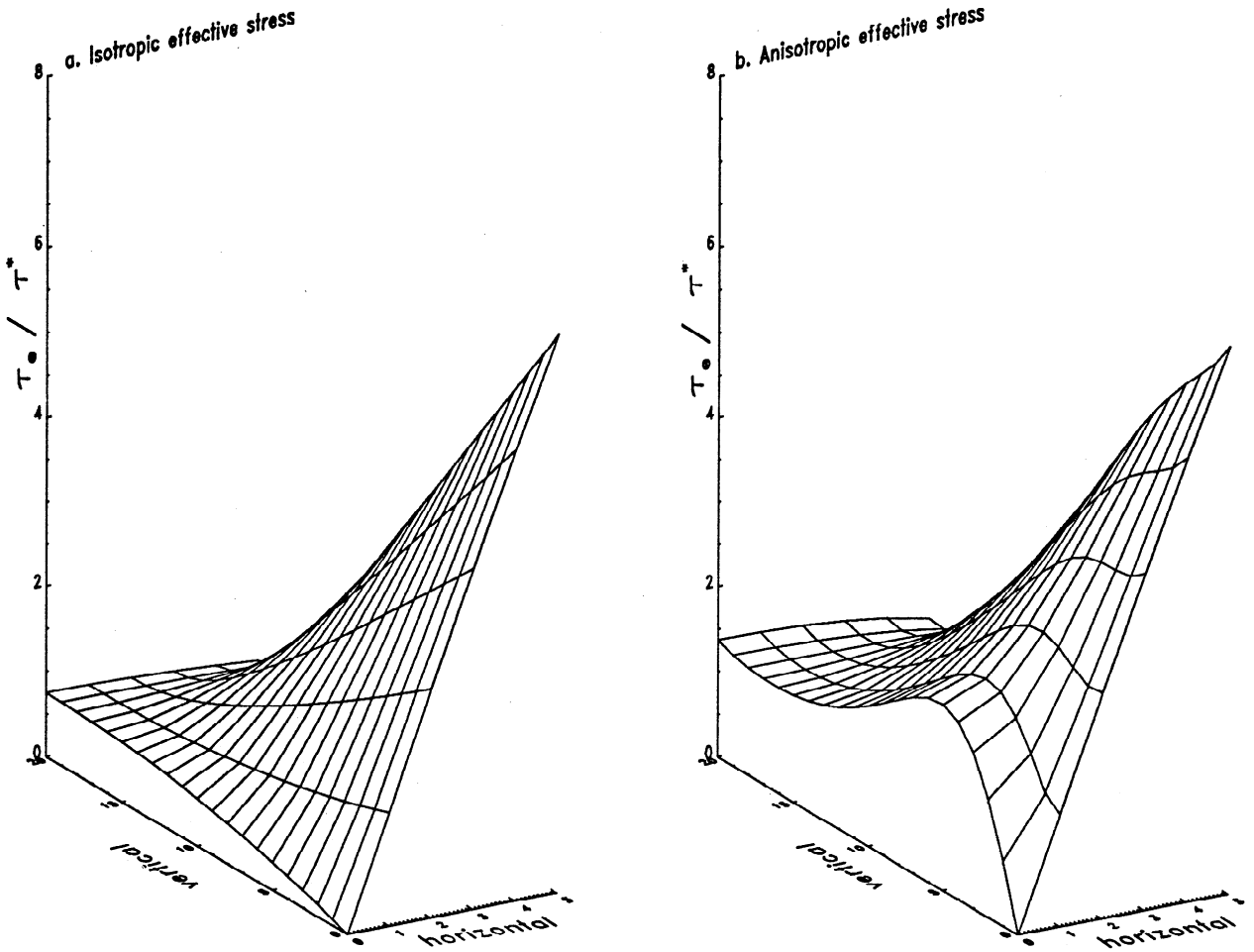

Figure 7. (a) Values for the isotropic case and (b) values for the anisotropic case. Values of the effective stress τ_e divided by τ^* in the domain $0 < z < H, 0 < x < 10$. The x axis represents the distance from the ice divide (point 0) to 10 (point 5), the y axis the depth from the surface (point 20) to the bottom (point 0) and the z axis the values of τ_e normalized by τ^*.

1. The accumulation rate to achieve steady state in the anisotropic case is more than 1.5 higher than the accumulation rate in the isotropic case. The motion of ice is globally accelerated in the anisotropic case compared to the isotropic situation, and the surface velocities are increased by a factor $\sim$ 1.7, 1.8 for the fabric used in this simulation.

2. Shearing is more concentrated for the lower parts of the ice sheet in the anisotropic case compared to the isotropic one.

3. The region where deformation is essentially due to longitudinal strain rate (i.e., the ice divide) is less extended in the anisotropic case. The domain where shear strain rate at the base is lower by 1 order of magnitude compared to the longitudinal strain rate at the surface is limited to $|x| < 8$ in the anisotropic case compared to $|x| < 10$ in the isotropic case.

4. At the ice divide, the shape of the stress tensor, compared with the rest of the ice sheet, is more singular for the anisotropic case than for the isotropic case.

The results of the last section refer to a single example involving specific shape, size, and rheology of the ice mass. Different surface elevation profiles lead to rather complex distributions of surface velocity, but the depth profiles of the velocity, strain rates, and stress components are not significantly affected. Also the value of the coefficient ψ_b affects the absolute value of the velocities but does not affect the depth profiles.

The use of the c axes distribution found in the GRIP site is only indicative. In fact, the topography of the bedrock is evidently not flat, and the ice flow is not isothermal. The ice flow is probably not strictly plane strain near the GRIP site, where the ice surface slopes radially outward [*Schott et al.*, 1992]. Furthermore, the fabric should slightly vary within the horizontal direction. Owing to these simplifications, our results cannot be directly used for climatic interpretation.

The complet description of strain-induced anisotropy has not been achieved in this work since the fabric at each grid point has not been actualized by the calculated velocity field. However, this work, which is a first step, gives a preliminary evaluation of the effect of the anisotropic behavior of ice on polar ice flow. This work allows confirmation and roughly estimation of the great influence of the anisotropic behavior of polar ice on the accuracy of ice flow model predictions. Results

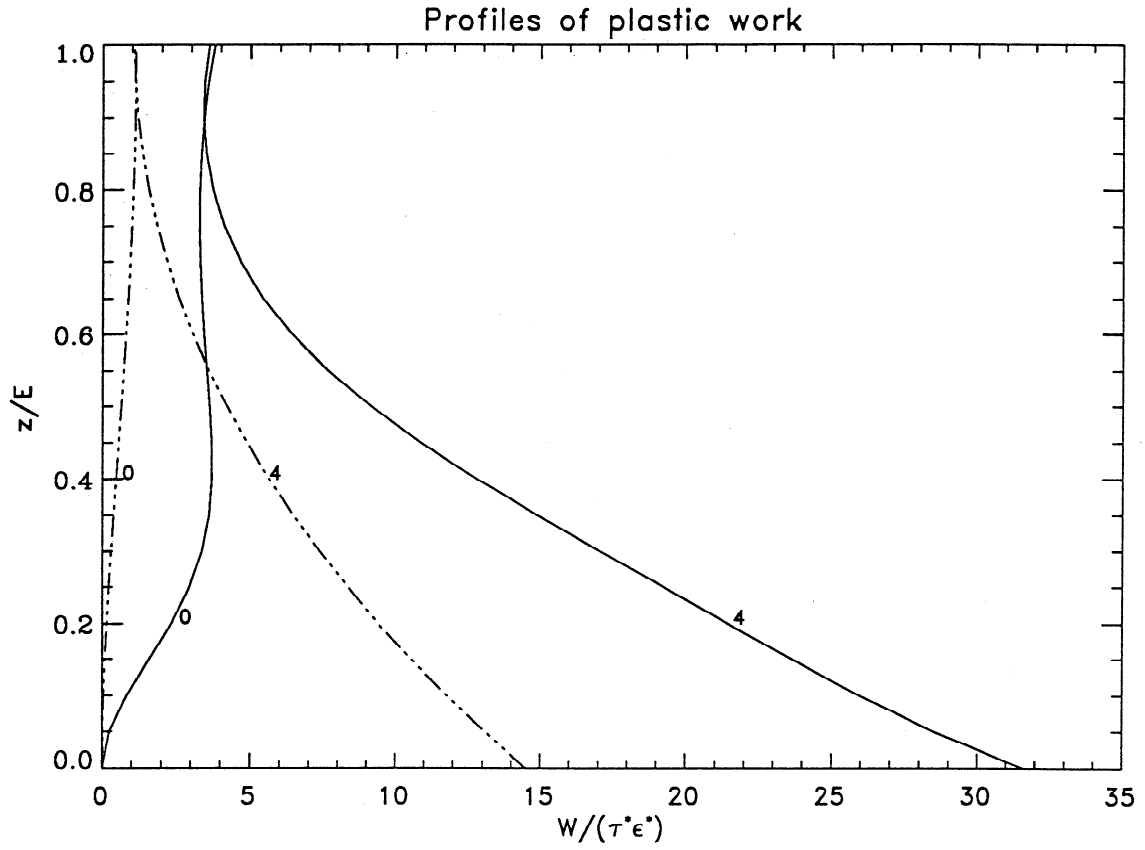

Figure 8. Profiles of plastic work, normalized by $\tau^*\epsilon^*$ versus normalized depth at the divide (0) and at 4 from the divide (4). Solid lines shows profiles for the anisotropic case, and dashed-dotted lines show profiles for the isotropic case.

show quantitatively, for the first time, that the very large viscoplastic anisotropy of polar ice must be taken into account in ice sheet flow modeling; it will significantly affect dating of the ice cores. The continuation of this work will concern: (1) the calculation with a non-Newtonian constitutive relation (i.e., $n = 3$), (2) the calculation of the temperature field which will on one hand accelerate the flow due to viscous heating and on the other hand will decelerate the flow due to the higher rate of advection of cold ice, and (3) the calculation of the surface evolution in steady state with a given accumulation rate.

Notation

The dimensional variables are indicated by a tilde, the corresponding dimensionless variables are noted with the same letter without a tilde.

a accumulation rate.
A_{ij} rheological parameters for stress sensitivity n=3.
$\tilde{B}$ temperature dependent factor in ice flow law.
B bedrock elevation.
B_b microscopic rheological parameter.
B_j rheological parameters for stress sensitivity n=3.
B_L bedrock elevation at the left edge of the domain.
B_R bedrock elevation at the right edge of the domain.
$\tilde{B}_0$ proportionality factor in ice flow law.
C rheological parameter for stress sensitivity $n = 3$.
$\tilde{\mathbf{D}}$, $\mathbf{D}$ strain rate tensor.
d_* typical ice thickness.
d_{ij} dimensionless strain rate normalized by ϵ^*.
E surface elevation.
E_L surface elevation at the left edge of the domain.
E_R surface elevation at the right edge of the domain.
F horizontal flux out of the domain.
g gravity acceleration.
H ice thickness.
h_0 height of the ice divide.
$\mathbf{I}$ identity tensor.
K_3 invariant of deviatoric stress tensor of degree 3.
L length of the domain.
$\mathcal{L}$ second order differential operator.
$\mathbf{M}$ dimensionless viscosity tensor.
n stress sensitivity.
$\mathbf{n}_s$ exterior unit normal vector at the surface.
$\tilde{p}$ fluid pressure.
$\tilde{p}'$, p' dynamic pressure.
p_{atm} dimensionless atmospheric pressure.

Q activation energy.
R gaz constant.
s_* typical stress.
s_{ij} dimensionless deviatoric stress tensor components normalized by τ^*.
$\tilde{\mathbf{S}}'$, $\mathbf{S}'$ deviatoric stress tensor.
S'_{ax} invariant of deviatoric stress tensor of degree 1.
t time.
$\tilde{T}$ temperature.
$\mathbf{u}$ velocity vector.
u_* typical accumulation rate or vertical velocity.
u_x horizontal velocity.
u_z vertical velocity.
$V(\theta)$ distribution of c axis.
$\dot{W}$ macroscopic rate of dissipation.
x horizontal coordinate.
x_L horizontal coordinate at the left edge of the domain.
x_R horizontal coordinate at the right edge of the domain.
$\tilde{z}$, z vertical coordinate.
Γ upper boundary of the domain.
Δt time step for the numerical iteration.
Δx space step.
ϵ^* dimensionless normalization factor for stain rate.
ζ horizontal coordinate equal to x.
η_0 isotropic viscosity.
η_{ij} directional viscosities.
θ angle between the c axis of one grain and the z axis.
$\theta_{1/2}$ median of θ.
ν coefficient of the c axis distribution.
ξ reduced depth.
ρ characteristic ice density.
$\tilde{\sigma}$, σ stress tensor.
τ^* dimensionless normalization factor for deviatoric stress.
$\tau_{\|}$, $\tau_{\perp}$ invariants of deviatoric stress tensor of degree 2.
τ_b resolved shear stress on the basal plane of the ice crystal.
$\tilde{\tau_e}$, τ_e effective stress.
ϕ, ψ dual macroscopic dissipation potential.
φ_i scalar fluidities.
ϕ_c microscopic dissipation potential.
ψ_b microscopic rheological parameter.
ψ_i rheological parameters for stress sensitivity n=1.

Acknowledgments. This work was supported by the PNEDC (Programme National d'Etude du Climat), the Environment program of the CCE, and the EISMINT program (European Science Foundation). We are grateful to L. Lliboutry, K. Hutter, R. B. Alley, and A. Salamatin for fruitful discussions.

References

Alley, R. B., Fabrics in polar ice sheets: development and prediction, *Science*, *240*, 493-495, 1988.

Alley, R. B., Flow-law hypotheses for ice sheet modeling, *J. Glaciol.*, *38*(129), 245-256, 1992.

Alley, R. B., A. J. Gow, and D. A. Meese, Mapping c-axis fabrics to study physical processes in ice, *J. Glaciol.*, *41*(137), 197-203, 1995.

Anandakrishnan, S., J. J. Fitzpatrick, R. B. Alley, A. J. Gow, and D. A. Meese, Shear-wave detection of asymmetric c-axis fabrics in the GISP2 ice core, *J. Glaciol.*, *40*(136), 491-496, 1994.

Andermann, I., Lois du comportement mecanique d'une glace roche anisotrope en regime stationnaire, these, Univ. Sci. et Med. de Grenoble, Grenoble, France, 1982.

Azuma N., A flow law for anisotropic ice and its application to ice sheets, *Earth Planet. Sci. Lett.*, *128*, 601-614, 1994.

Budd, W. F., and T. H. Jacka, A review of ice rheology for ice sheet modelling, *Cold Reg. Sci. Technol.*, *16*, 107-144, 1989.

Canova, G. R., U. F. Kocks, C. N. Tome, and J. J. Jonas, The yield surface of textured polycrystals, *J. Mech. Phys. Solids*, *33*(4), 371-397, 1985.

Castelnau, O., Modelisation du comportement mecanique de la glace polycristalline par une approche auto-coherente; application du developpement de textures dans les glaces des calottes polaires, these, Univ. J. Fourier, Grenoble, France, 1996.

Castelnau, O., and P. Duval, Simulations of anisotropy and fabric development in polar ices, *Ann. Glaciol.*, *20*, 277-282, 1994.

Castelnau, O., P. Duval, R. A. Lebensohn, and G. R. Canova, Viscoplastic modeling of texture development in polycrystalline ice with a self-consistent approach: Comparison with bound estimates, *J. Geophys. Res.*, *101*, 13,851-13,868, 1996a.

Castelnau, O., T. Thorsteinsson, J. Kipfstuhl, P. Duval, and G. R. Canova, Modelling fabric development along the GRIP ice core (central Greenland), *Ann. Glaciol.*, *23*, in press, 1996b.

Chorin, A. J., A numerical method for solving incompressible viscous flow problems, *J. Comput. Phys.*, *2*, 12-26, 1967.

Dahl-Jensen, D., Determination of the flow properties at Dye 3, south Greenland, by bore-hole-tilting measurements and perturbation modelling, *J. Glaciol.*, *31*(108), 92-98, 1985.

Dahl-Jensen, D., Two dimensional thermomechanical modelling of flow and depth-age profiles near the ice divide in central Greenland, *Ann. Glaciol.*, *12*, 31-36, 1989a.

Dahl-Jensen, D., Steady thermomechanical flow along two-dimensional flow lines in large grounded ice sheets, *J. Geophys. Res.*, *94*, 10,355-10,362, 1989b.

Doake, C. S. M., and E. W. Wolff, Flow law for ice in polar ice sheets, *Nature*, *314*(6008), 255-257, 1985.

Duval, P., and O. Castelnau, Dynamic recrystallization of ice in polar ice sheets, *J. Phys. IV*, Colloque C3, *5*, 197-205, 1995.

Duval, P., M. F. Ashby, and I. Andermann, Rate-controlling processes in the creep of polycrystalline ice, *J. Phys. Chem.*, *87*(21), 4066-4074, 1983.

Fujita, S., M. Nakawo, and S. Mae., Orientation of the 700m Mizuho core and its strain history, paper presented at the Ninth Symposium on Polar Meteorology and Glaciology, National Institute of Polar Research, Tokyo, 1987.

Gow, A. J., and T. Williamson, Rheological implications of the internal structure and crystal fabrics of the West Antarctic ice sheet as revealed by deep core drilling at Byrd Station, *CRREL Rep. 76-35*, 25 pp., 1976.

Herron, S.L., C.C. Langway Jr., and K. A. Brugger, Ultrasonic velocities and crystalline anisotropy in the ice core from Dye 3, Greenland, in *Greenland ice core: Geophysices, Geochemistry, and the Environment, Geophys.*

Monogr. Ser., vol. 33, edited by C.C. Langway Jr., H. Oeschger, and W. Dansgaard, pp. 23-31, AGU, Washington, D. C., 1985.

Hill, R., Constitutive dual potentials in classical plasticity, *J. Mech. Phys. Solids*, *33*(4), 371-397, 1987.

Hindmarsh, R. C. A., and K. Hutter, Numerical fixed domain solution of free-surface flows coupled with an evolving interior field, *Int. J. Numer. Anal. Methods Geomech.*, *12*, 437-459, 1988.

Hooke, R. L., Flow law for polycrystalline ice in glaciers: Comparison of theoretical predictions, laboratory data, and field measurements, *Rev. Geophys.*, *19*(4), 664-672, 1981.

Hutchinson, J.W., Bounds and self-consistent estimates for creep of polycrystalline materials, *Proc. R. Soc. London A*, *348*, 101-127, 1976.

Hutter, K., *Theoretical Glaciology: Material Science of Ice and the Mechanics of Glaciers and Ice Sheets*, D. Reidel, Norwell Mass., 1983.

Kostecka, J. M., and I. M. Whillans, Mass balance along two transects of wide side of the Greenland ice-sheet, *J. Glaciol.*, *34*, 31-39, 1988.

Lemaitre, J., and J. L. Chaboche, *Mechanics of Solid Materials*, Cambridge Univ. Press, New York, 1990.

Lile, R. C., The effect of anisotropy on the creep of polycrystalline ice, *J. Glaciol.*, *21*(85), 475-483, 1978.

Lipenkov, V. Y., N. I. Barkov, P. Duval, and P. Pimenta, Crystalline texture of the 2083 m ice core at Vostok Station, Antarctica, *J. Glaciol.*, *35*(121), 392-398, 1989.

Lliboutry L., Anisotropic, transversally isotropic nonlinear viscosity of rock ice and rheological parameters inferred from homogenization, *Int. J. Plast.*, *9*, 619-632, 1993.

Lliboutry, L., and P. Duval, Various isotropic and anisotropic ices found in glaciers and polar ice caps and their corresponding rheologies, *Ann. Geophys.*, *3*(2), 207-224, 1985.

Mangeney, A., Modelisation de l'ecoulement de la glace dans les calottes polaires: Prise en compte d'une loi de comportement anisotrope, these, Univ. P. et M. Curie, Paris, France, 1996.

Morland, L. W., Thermomechanical balances of ice sheet flows, *Geophys. Astrophys. Fluid Dyn.*, *29*, 237-266, 1984.

Nye, J. F., The mechanics of glacier flow, *J. Glaciol.*, *2*(12), 82-93, 1952.

Nye, J. F., The distribution of stress and velocity in glaciers and ice-sheets, *Proc. R. Soc. London, Ser. A*, *239*, 113-133, 1957.

Patankar, S. V., *Numerical heat transfer and fluid flow, Ser. Comput. Phys. Processes Mech. Therm. Sci.*, Taylor and Francis, Bristol, Pa., 1980.

Paterson, W. S. B., and E. D. Waddington, Past precipitation rates derived from ice core measurements: Methods and data analysis, *Rev. Geophys.*, *22*(2), 123-130, 1984.

Peyret, R., and T. D. Taylor, *Computational Methods in Fluid Flows*, Springer-Verlag, New York, 1983.

Pimienta, P., and P. Duval., Rate controlling processes in the creep of polar ice, *J. Phys. C1*, suppl. 3, *48*, 243-248, 1987.

Pimienta, P., and P. Duval., Mechanical behavior of ice along the 2040m Vostok core, Antarctica, *Ann. Glaciol.*, *10*, 137-140, 1988.

Raymond, C. F., Deformation in the vicinity of ice divides, *J. Glaciol.*, *29*(103), 357-373, 1983.

Reeh, N., A flow-line model for calculating the surface profile and the velocity, strain-rate, and stress fields in an ice-sheet, *J. Glaciol.*, *34*(116), 46-54, 1988.

Russel-Head, D. S., and W. F. Budd, Ice-sheet flow properties derived from bore-hole shear measurements combined with ice core studies, *J. Glaciol.*, *24*(90), 117-130, 1979.

Schott, C., E. D. Waddington and C. F. Raymond, Predicted time-scales for GISP2 and GRIP boreholes at Summit, Greenland, *J. Glaciol.*, *38*(128), 162-168, 1992.

Schott Hvidberg, C., Steady state thermo-mechanical modelling of ice flow near the center of large ice sheets with the finite element technique, *Ann. Glaciol.*, *23*, in press, 1996.

Shoji, H., and C. C. Langway, Flow behavior of basal ice as related to modelling considerations, *Ann. Glaciol.*, *5*, 141-148, 1984.

Shoji, H. and C. C. Langway, Mechanical properties of fresh ice core from Dye 3, Greenland, in *Greenland Ice Core: Geophysics, Geochemistry, and the Environment, Geophys. Monogr. Ser.*, vol. 33, edited bye C. C. Langway Jr., H. Oeschger, and W. Dansgaard, pp. 39-48, AGU, Washington, D. C., 1988.

Sotiropoulos, F., and S. Abdallah, The discrete continuity equation in primitive variable solutions of incompressible flow, *J. Comput. Phys.*, *95*, 212-227, 1991.

Szidarovsky, F., K. Hutter, and S. Yakowitz, Computational ice-divide analysis of a cold plane ice sheet under steady conditions, *Ann. Glaciol.*, *12*, 170-177, 1989.

Tafti, D., Alternate formulation for the pressure equation laplacian on a collocated grid for solving the unsteady incompressible Navier-Stokes equations, *J. Comput. Phys.*, *116*, 143-153, 1995.

Thorsteinsson, T., J. Kipfsuhl, and H. Miller, Textures and fabrics in the GRIP ice core, *J. Geophys. Res.*, in press, 1996.

Van der Veen, C. J., and I. M. Whillans, Development of fabric in ice, *Cold Reg. Sci. Technol.*, *22*, 171-195, 1994.

Van Houtte, P., Application of plastic potentials to strain rate sensitive and insensitive anisotropic materials, *Int. J. Plast.*, *10*(7), 719-748, 1994.

Waddington, E. D., D. A. Fisher, R. M. Koerner, and W. S. B. Paterson, Flow near an ice divide: Analysis problems and data requirements, *Ann. Glaciol.*, *8*, 171-174, 1985.

Ziegler, H., *An Introduction to Thermomechanics*, North-Holland, New York, 1977.

F. Califano, Scuola Normale Superiore (INFM-FORUM), Piazza dei Cavalieri 7, 56100, Pisa, Italy. (e-mail: califano@cibs.sns.it)

O. Castelnau, LPMTM-CNRS, Universite Paris-Nord, Institut Galilee, av. J. B. Clement, 93430 Villetaneuse, France. (e-mail: oc@lpmtm.univ-paris13.fr)

A. Mangeney, Laboratoire de Glaciologie et Geophysique de l'environnement, CNRS, 54, rue Moliere, 38402 Saint Martin d'Heres, France. (e-mail: nan@glaciog.grenet.fr)

(Received November 14, 1995; revised April 8, 1996; accepted June 4, 1996.)